Supporting Information

Precursor Gene Engineering Expands the Loop Region of the Lasso Peptide Microcin J25

Hui-Ni Tan[1], Julian D. Hegemann[23], Manuel Maestre-Reyna[14], John Chu[15]*

[1]Department of Chemistry, National Taiwan University, Taipei 106319, Taiwan. [2]Institute of Pharmaceutical Biology, Technische Universität Braunschweig, Braunschweig, Germany. [3]Center of Pharmaceutical Engineering (PVZ), Technische Universität Braunschweig, Braunschweig, Germany. [4]Institute of Biological Chemistry, Academia Sinica, Taipei 115024, Taiwan. [5]Center for Emerging Material and Advanced Devices, National Taiwan University, Taipei 106319, Taiwan.

*Correspondence: johnchu@ntu.edu.tw

Table of Contents

MATERIALs and METHODs

Reagents, Media, and Strains

All microcin J25 (MccJ25) variants described herein were derived from the wild-type (WT) biosynthetic gene cluster (BGC) in the pTUC202 plasmid.[1] The MccJ25 BGC encodes four genes, *mcjA*, *mcjB*, *mcjC*, and *mcjD*. DNA primers for cloning and sequencing were purchased from Genomics BioSci & Technology Company (Taiwan) and are listed in Table S1. Reagents and kits for site-directed mutagenesis (E0554) were purchased from New England Biolabs (USA). Other reagents were purchased from BioShop Canada Inc. (Canada). Constructs described herein have all been verified by Sanger sequencing by Genomics BioSci & Technology Company (Taiwan). Cloning was carried out in *Escherichia coli* DH5α grown in Luria-Bertani (LB) medium supplemented with chloramphenicol (25 μg/mL). MccJ25 production was performed in *E. coli* BL21(DE3) grown in M9 medium supplemented with chloramphenicol (25 μg/mL).

MccJ25 Production

Procedure for MccJ25 production is based on a previous publication[2] and slightly modified as follows. A single *E. coli* BL21(DE3) colony harboring pTUC202 with the WT or engineered MccJ25 BGC was inoculated into LB medium (3 mL) supplemented with chloramphenicol (25 μg/mL) and grown at 37 °C overnight. This starter culture was diluted to OD_{600} 0.1 in M9 medium (50 mL) supplemented with chloramphenicol (25 μg/mL) and grown at 37 °C for 4 days. On day 5 the cells were removed by centrifugation; 8 mL of the supernatant was extracted with 1 volume of 1-butanol and the organic layer was collected and dried under reduced pressure. The crude extract was redissolved in H_2O (1 mL) and immediately subjected to HPLC analysis for quantification, mass spectrometry (MS) analysis for structure determination, and growth inhibition zone assay for antibacterial activity evaluation. All MccJ25 variants were carried out in the same way (*Figure S1 – S14*).

Confirmation by MALDI-MS and Quantification by HPLC

As described in our previous publication,[3] HPLC analysis was performed on a Waters Instrument (996 UV detector, 600 pump and controller) equipped with an analytical Thermo Scientific™ C18 column (Hypersil GOLD™, 250 x 4.6 mm, 175 Å, 5 μm) using a two-solvent system. Water and acetonitrile supplemented with 0.1% (v/v) formic acid were used as the mobile phase, designated as solvent A and B, respectively. The following program was used: 0 – 5 min (10%B, isocratic), 5 – 25 min (10 to 50%B, linear gradient), 25 – 26 min (50 to 90%B, linear

gradient), 26 – 30 min (90%B, isocratic). The flow rate was fixed at 1 mL/min and the absorbance at 210-450 nm was recorded. MccJ25 variants typically eluted between 22-27 min; the peak for every variant was collected and confirmed by MALDI-TOF MS (microTOF-QII, Bruker).

Based on the following procedure, biological triplicates (n = 3) were performed for every MccJ25 variant to quantitate the production yield and reported as the average ± standard deviation in the main text (Table 1):

1) Calculate the extinction coefficient (ε) of each MccJ25 variant at 214 nm using the *BeStSel Extinction Coefficient Calculation* (https://bestsel.elte.hu/extcoeff.php), which is one of many servers that are freely available for this purpose.
2) Obtain the 8 mL crude extract of a MccJ25 variant from 50 mL of culture based on the *MccJ25 Production* procedure described above.
3) Dissolve the crude extract in 1 mL of water.
4) Mix 95 μL the solution with 5 μL of caffeine (2 mg/mL) and co-inject into HPLC.
5) The peak that corresponds to the MccJ25 variant (confirmed by MALDI-MS) at 214 nm was integrated and compared to that of the internal standard (100 μg/mL of caffeine in every injection).
6) Production yield of variant *X* was estimated based on the equation below:

$$\text{Yield}_X = \frac{\text{Peak}_X}{\text{Peak}_{\text{Caffeine in X}}} \times \overline{\left(\frac{\text{Peak}_{\text{Caffeine in MccJ25}}}{\text{Peak}_{\text{MccJ25}}}\right)} \times \frac{\varepsilon_{\text{MccJ25}}}{\varepsilon_X} \times \overline{\text{Yield}}_{\text{MccJ25}}$$

Lasso Topology Determination by MS

Topology determination was performed by incubating MccJ25 variant crude extracts (26 μL) with 40 μg/mL of thermolysin in 0.14 M NH_4HCO_3 buffer at pH 8.0 (100 μL in total) under 46°C for 1 to 5 h. Reaction was quenched by adding 25 μL of acetic acid and the resulting peptide mixtures were subjected to MALDI-TOF MS (microTOF-QII, Bruker) analysis. The presence of a string trapped within the ring is indicative of the lasso topology prior to thermolysin digestion (*Figure S1 – S14*).

Growth Inhibition Zone Assay

A single colony of *E. coli* MG1655 was inoculated into LB medium (3 mL) and grown at 37 °C overnight. The culture was then diluted 100-fold into 10 mL of molten M9 agar and poured into a

petri dish and left to solidify. Crude extracts obtained from 100 mL of MccJ25 production culture were resuspended in 1 mL of H_2O. Once the M9/agar mixture solidified, 1, 5, 10, 20, and 30 μL of the crude extracts of MccJ25 variants were spotted onto the surface. The petri dishes were then incubated at 37°C for 16 h. The antibacterial activity of each variant was quantitated based on the equation below and reported as a score relative to that of WT MccJ25 (Table 1):

$$\text{score} = \frac{d^2}{\text{volume} \times \text{yield}}$$

McjC Structure Prediction and Cavity Volume Calculation

The AlphaFold Server[4-5] was used for protein structure prediction. We first predicted the structures of McjB and McjC individually, and then the McjA/McjB/McjC ternary complex structure prediction was carried out by submitting three protein sequences simultaneously. The predicted protein complex structures were rendered using the PyMOL Molecular Graphics System, v.3.1 (Schrödinger LLC, USA).

The cavity of McjC was calculated by using the CASTpFold (Computed Atlas of Surface Topography of the universe of protein Folds) analysis server.[6-7] The predicted McjC structure was submitted into the server in pdb format, and the probe radius was set as the approximate size of water molecules (r = 1.4 Å). The measurement was also visualized by using the PyMOL Molecular Graphics System with CASTpFold pocket loader plugin.

SUPPLEMENTARY FIGUREs

Figure S1. The HPLC analysis and MS confirmation of wild-type MccJ25

Wild-type MccJ25. **a)** Crude extract was analyzed by HPLC with MccJ25 eluted at t_R = 26.2 min. **b)** The peak presumed to be MccJ25 was collected and confirmed by MALDI-TOF MS with the observed m/z 2129.103 and 2145.095 as the sodium and potassium adduct $[M+Na]^+$ and $[M+K]^+$, respectively. **c)** Thermolysin digestion with single cleavage as the result lead to the hydrolysis of MccJ25, with the observed m/z 2147.307 and 2163.300 as the sodium and potassium adduct $[M+H_2O+Na]^+$ and $[M+H_2O+K]^+$, respectively.

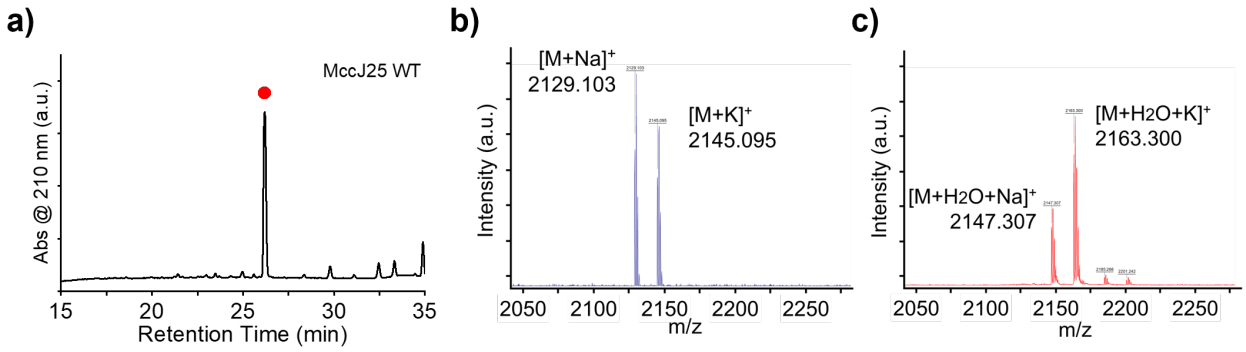

Figure S2. The HPLC analysis and MS confirmation of MccJ25 $^{R}A_1$ variant

MccJ25 $^{R}A_1$ variant. **a)** Crude extract was analyzed by HPLC with $^{R}A_1$ variant eluted at t_R = 26.2 min. **b)** The peak presumed to be $^{R}A_1$ variant was collected and confirmed by MALDI-TOF MS with the observed m/z 2178.116 and 2202.071 as the hydrogen and potassium adduct $[M+H]^+$ and $[M+K]^+$, respectively. **c)** Thermolysin digestion of $^{R}A_1$ variant result in only partial peptide m/z being observed, with 1108.806 as sodium adduct $[Ring+YF+Na]^+$ and 1280.069 as potassium adduct $[Ring+YFVG+K]^+$, indicated $^{R}A_1$ variant as a branched-cyclic peptide as the loop region of peptide was not mechanically locked within the ring region.

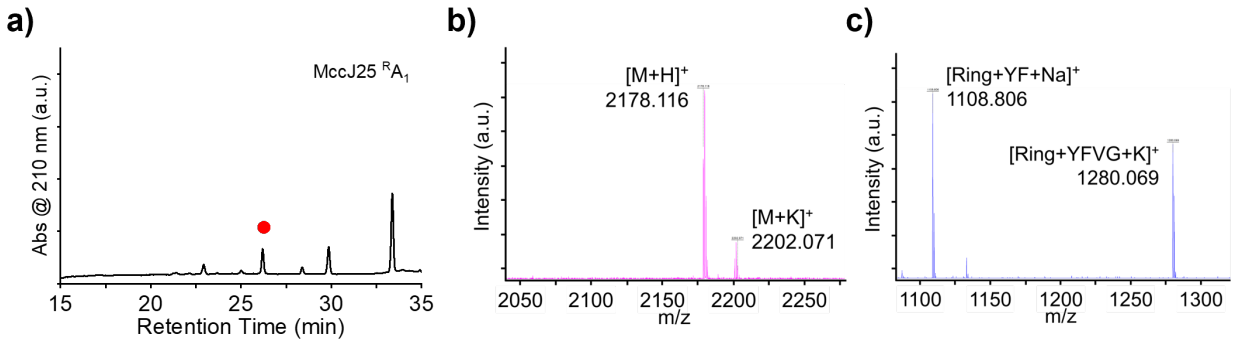

Figure S3. The HPLC analysis and MS confirmation of MccJ25 $^{T}G_1$ variant.

MccJ25 $^{T}G_1$ variant. **a)** Crude extract was analyzed by HPLC with $^{T}G_1$ variant eluted at t_R = 25.8 min. **b)** The peak presumed to be $^{T}G_1$ variant was collected and confirmed by MALDI-TOF MS with the observed m/z 2186.792 and 2202.888 as the sodium and potassium adduct $[M+Na]^+$ and $[M+K]^+$, respectively. The lasso topology of this variant was confirmed in a previous publication.[8]

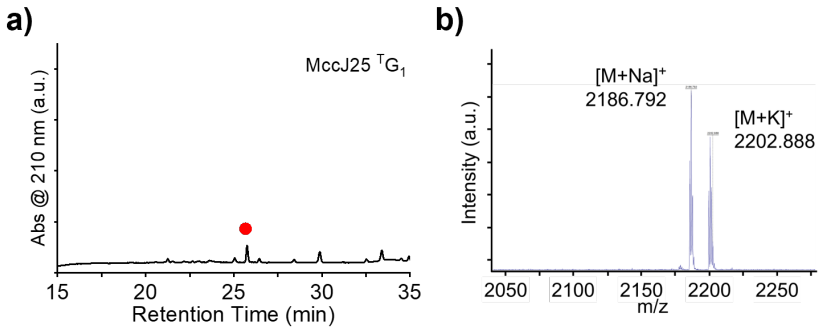

Figure S4. The HPLC analysis and MS confirmation of MccJ25 $^{L}A_1$ variant.

MccJ25 $^{L}A_1$ variant. **a)** Crude extract was analyzed by HPLC with $^{L}A_1$ variant eluted at t_R = 26.3 min. **b)** The peak presumed to be $^{L}A_1$ variant was collected and confirmed by MALDI-TOF MS with the observed m/z 2200.379 and 2216.406 as the sodium and potassium adduct $[M+Na]^+$ and $[M+K]^+$, respectively. **c)** Thermolysin digestion with single cleavage as the result lead to the hydrolysis of $^{L}A_1$ variant, with the observed m/z 2218.223 and 2234.200 as the sodium and potassium adduct $[M+H_2O+Na]^+$ and $[M+H_2O+K]^+$, respectively.

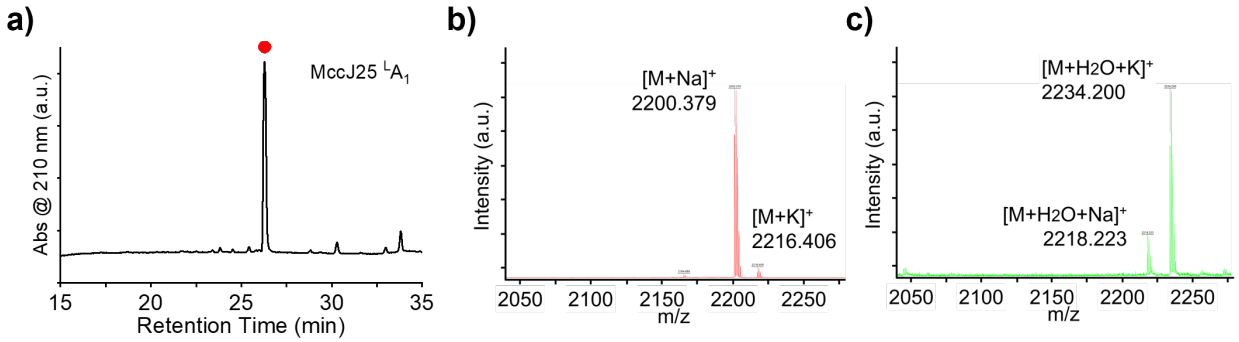

Figure S5. The HPLC analysis and MS confirmation of MccJ25 $^{L}A_3$ variant

MccJ25 $^{L}A_3$ variant. **a)** Crude extract was analyzed by HPLC with $^{L}A_3$ variant eluted at t_R = 26.8 min. **b)** The peak presumed to be $^{L}A_3$ variant was collected and confirmed by MALDI-TOF MS with the observed m/z 2342.916 as the sodium adduct $[M+Na]^+$. **c)** Thermolysin digestion led to the loss of a pentapeptide fragment "VGAAA", resulting in a supramolecular complex, also known as a [2]rotaxane [(GGAHGVPEYF)•(IGTPISFYG)], with the observed m/z 1991.392 as the sodium adduct $[M\text{-}VGAAA+H_2O+Na]^+$.

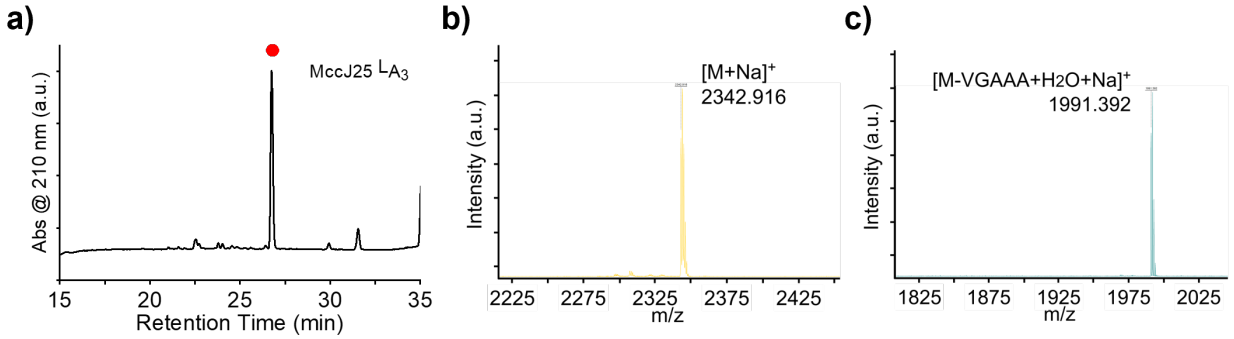

Figure S6. The HPLC analysis and MS confirmation of MccJ25 $^{L}A_5$ variant

MccJ25 $^{L}A_5$ variant. **a)** Crude extract was analyzed by HPLC with $^{L}A_5$ variant eluted at t_R = 25.7 min. **b)** The peak presumed to be $^{L}A_5$ variant was collected and confirmed by MALDI-TOF MS with the observed m/z 2484.254 and 2500.317 as the sodium and potassium adduct $[M+Na]^+$ and $[M+K]^+$, respectively. **c)** Thermolysin digestion led to the loss of a heptapeptide fragment "VGAAAAA", resulting in a supramolecular complex, also known as a [2]rotaxane [(GGAHGVPEYF)•(IGTPISFYG)], with the observed m/z 1991.293 and 2007.292 as the sodium and potassium adduct $[M\text{-}VGA_5+H_2O+Na]^+$ and $[M\text{-}VGA_5+H_2O+K]^+$, respectively.

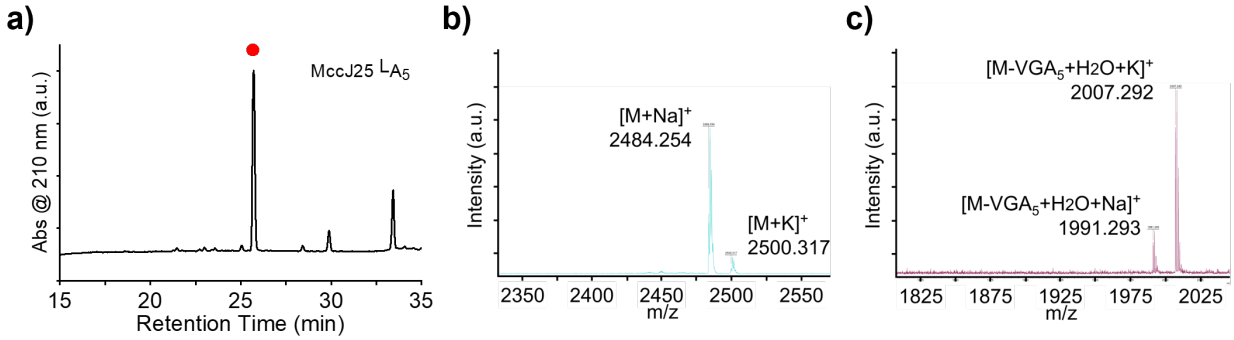

Figure S7. The HPLC analysis and MS confirmation of MccJ25 $^{L}A_7$ variant

MccJ25 $^{L}A_7$ variant. **a)** Crude extract was analyzed by HPLC with $^{L}A_7$ variant eluted at t_R = 26.0 min. **b)** The peak presumed to be $^{L}A_7$ variant was collected and confirmed by MALDI-TOF MS with the observed m/z 2626.830 and 2642.882 as the sodium and potassium adduct $[M+Na]^+$ and $[M+K]^+$, respectively. **c)** Thermolysin digestion led to the loss of a nonapeptide fragment "VGAAAAAAA", resulting in a supramolecular complex, also known as a [2]rotaxane [(GGAHGVPEYF)•(IGTPISFYG)], with the observed m/z 1991.292 and 2007.259 as the sodium and potassium adduct $[M\text{-}VGA_7+H_2O+Na]^+$ and $[M\text{-}VGA_7+H_2O+K]^+$, respectively.

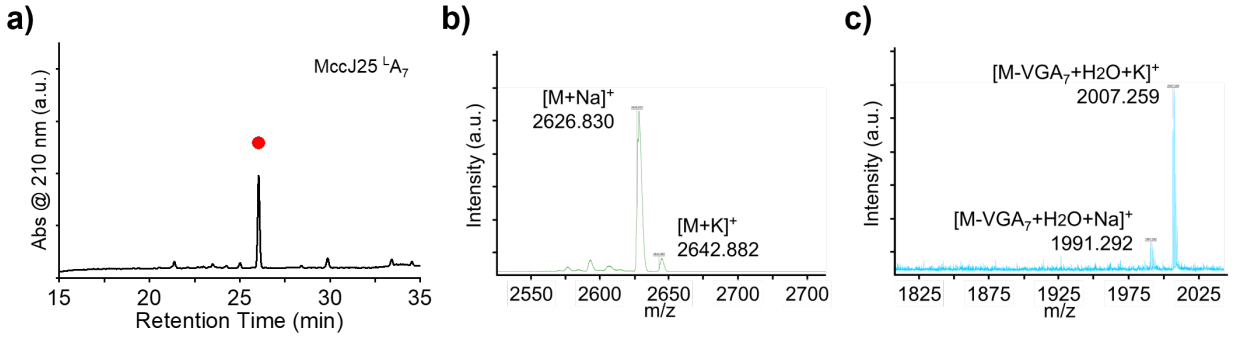

Figure S8. The HPLC analysis and MS confirmation of MccJ25 $^{L}A_{10}$ variant

MccJ25 $^{L}A_{10}$ variant. **a)** Crude extract was analyzed by HPLC with $^{L}A_{10}$ variant eluted at t_R = 26.4 min. **b)** The peak presumed to be $^{L}A_{10}$ variant was collected and confirmed by MALDI-TOF MS with the observed m/z 2839.305 and 2855.306 as the sodium and potassium adduct $[M+Na]^+$ and $[M+K]^+$, respectively. **c)** Thermolysin digestion led to the loss of an octapeptide fragment "VGAAAAAA", resulting in a supramolecular complex, also known as a [2]rotaxane [(GGAHGVPEYF)•(IGTPISFYG)], with the observed m/z 2275.170 and 2292.923 as the sodium and potassium adduct $[M\text{-}VGA_6+H_2O+Na]^+$ and $[M\text{-}VGA_6+H_2O+K]^+$, respectively.

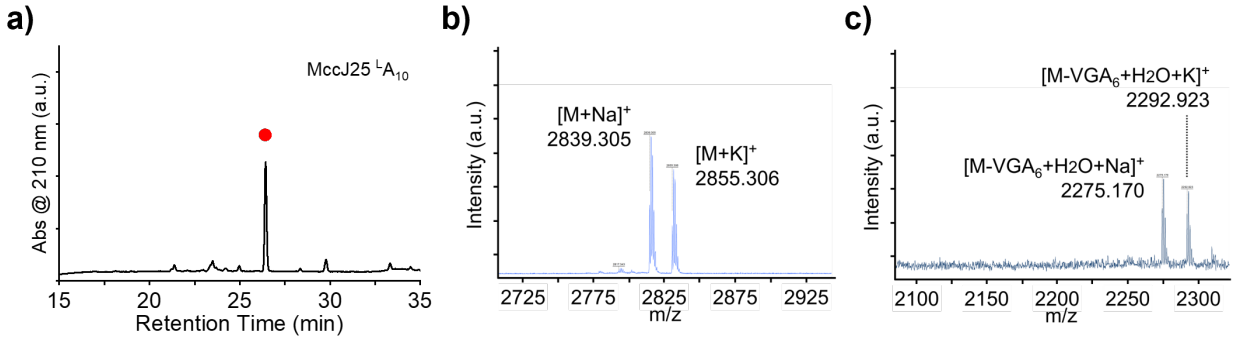

Figure S9. The HPLC analysis and MS confirmation of MccJ25 $^{L}G_{10}$ variant

MccJ25 $^{L}G_{10}$ variant. **a)** Crude extract was analyzed by HPLC with $^{L}G_{10}$ variant eluted at t_R = 23.3 min. **b)** The peak presumed to be $^{L}G_{10}$ variant was collected and confirmed by MALDI-TOF MS with the observed m/z 2699.992 and 2715.974 as the sodium and potassium adduct $[M+Na]^+$ and $[M+K]^+$, respectively. **c)** Thermolysin digestion with single cleavage as the result lead to the hydrolysis of $^{L}G_{10}$ variant, with the observed m/z 2695.197, 2717.199 and 2733.194 as the hydrogen, sodium and potassium adduct $[M+H_2O+H]^+$, $[M+H_2O+Na]^+$ and $[M+H_2O+K]^+$, respectively.

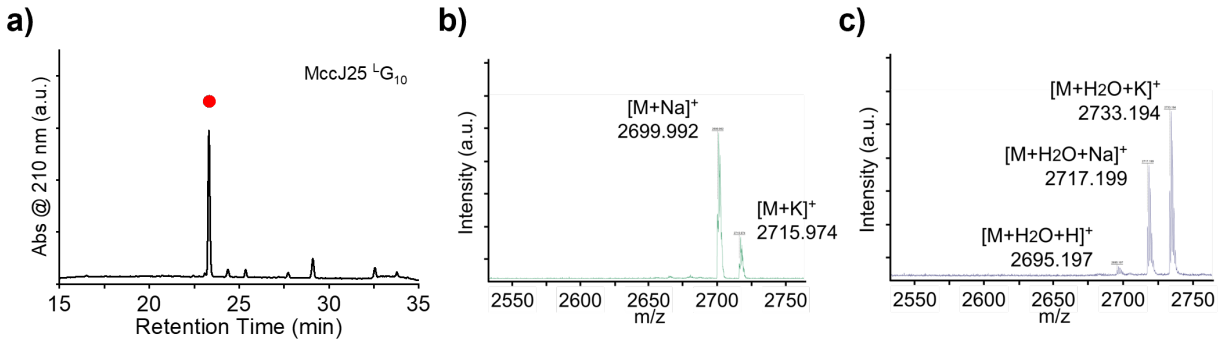

Figure S10. The HPLC analysis and MS confirmation of MccJ25 $^{L}G_{15}$ variant

MccJ25 $^{L}G_{15}$ variant. **a)** Crude extract was analyzed by HPLC with $^{L}G_{15}$ variant eluted at t_R = 22.9 min. **b)** The peak presumed to be $^{L}G_{15}$ variant was collected and confirmed by MALDI-TOF MS with the observed m/z 2962.345, 2984.305 and 3000.301 as the hydrogen, sodium and potassium adduct $[M+H]^+$, $[M+Na]^+$ and $[M+K]^+$, respectively. **c)** Thermolysin digestion with single cleavage as the result lead to the hydrolysis of $^{L}G_{15}$ variant, with the observed m/z 3002.322 and 3018.306 as the sodium and potassium adduct $[M+H_2O+Na]^+$ and $[M+H_2O+K]^+$, respectively.

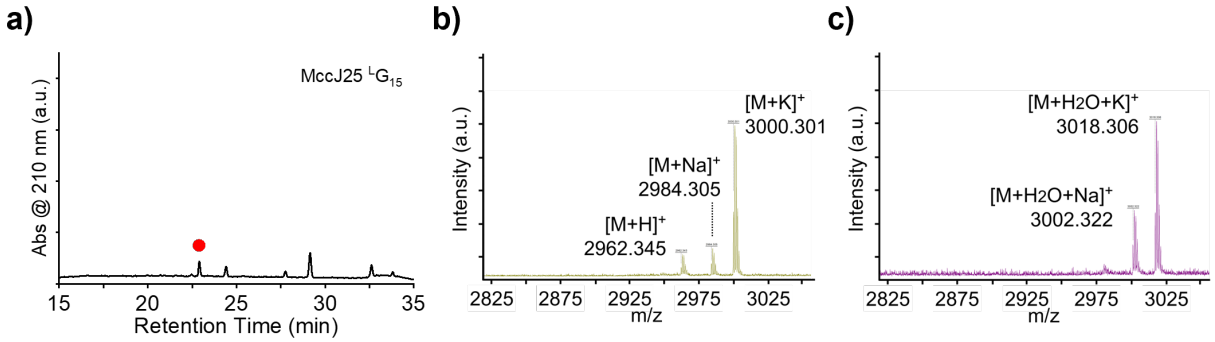

Figure S11. The HPLC analysis and MS confirmation of MccJ25 $^{L}A_1A_1$ variant

MccJ25 $^{L}A_1A_1$ variant. **a)** Crude extract was analyzed by HPLC with $^{L}A_1A_1$ variant eluted at t_R = 24.8 min. **b)** The peak presumed to be $^{L}A_1A_1$ variant was collected and confirmed by MALDI-TOF MS with the observed m/z 2271.678 and 2287.667 as the sodium and potassium adduct $[M+Na]^+$ and $[M+K]^+$, respectively. **c)** Thermolysin digestion led to the loss of a tripeptide fragment "VAG", resulting in a supramolecular complex, also known as a [2]rotaxane [(GGAHGVPEYF)•(IGTPAISFYG)], with the observed m/z 2040.335 and 2062.359 as the hydrogen and sodium adduct $[M\text{-}VAG+H_2O+H]^+$ and $[M\text{-}VAG+H_2O+Na]^+$, respectively.

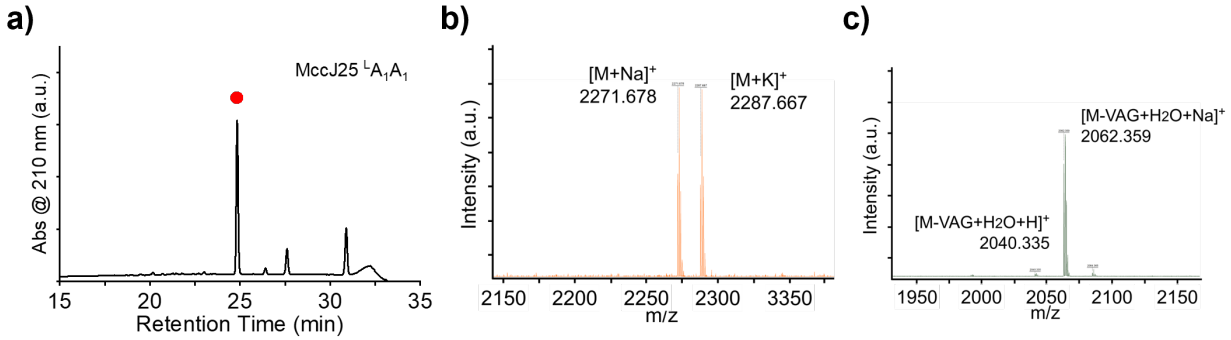

Figure S12. The HPLC analysis and MS confirmation of MccJ25 ^{L}ARA variant

MccJ25 ^{L}ARA variant. **a)** Crude extract was analyzed by HPLC with ^{L}ARA variant eluted at t_R = 23.3 min. **b)** The peak presumed to be ^{L}ARA variant was collected and confirmed by MALDI-TOF MS with the observed m/z 2405.550 and 2427.554 as the hydrogen and sodium adduct $[M+H]^+$ and $[M+Na]^+$, respectively. **c)** Thermolysin digestion led to the loss of a pentapeptide fragment "VGARA", resulting in a supramolecular complex, also known as a [2]rotaxane [(GGAHGVPEYF)•(IGTPISFYG)], with the observed m/z 1991.280 and 2007.293 as the sodium and potassium adduct $[M\text{-VGARA}+H_2O+Na]^+$ and $[M\text{-VGARA}+H_2O+K]^+$, respectively.

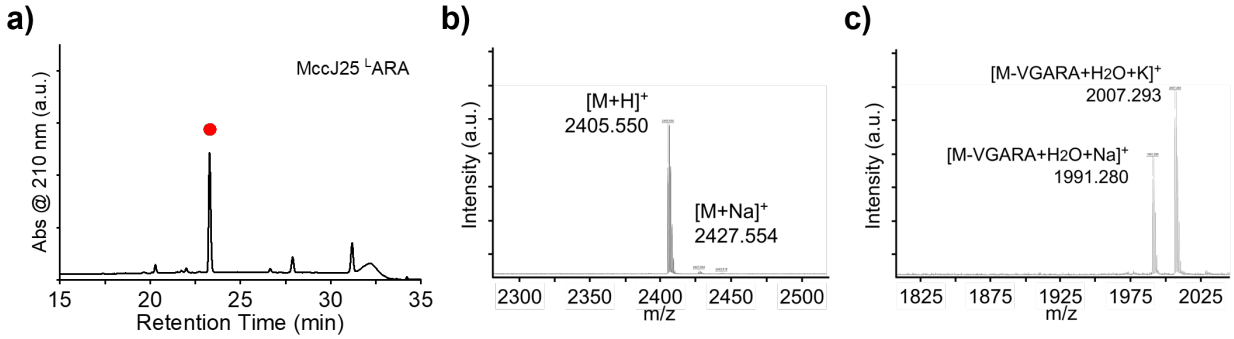

Figure S13. The HPLC analysis and MS confirmation of MccJ25 ^{L}SARAE variant

MccJ25 ^{L}SARAE variant. **a)** Crude extract was analyzed by HPLC with ^{L}SARAE variant eluted at t_R = 22.8 min. **b)** The peak presumed to be ^{L}SARAE variant was collected and confirmed by MALDI-TOF MS with the observed m/z 2621.640 and 2643.866 as the hydrogen and sodium adduct $[M+H]^+$ and $[M+Na]^+$, respectively. **c)** Thermolysin digestion led to the loss of a heptapeptide fragment "VGSARAE", resulting in a supramolecular complex, also known as a [2]rotaxane [(GGAHGVPEYF)•(IGTPISFYG)], with the observed m/z 1991.238 and 2007.237 as the sodium and potassium adduct $[M\text{-VGSARAE}+H_2O+Na]^+$ and $[M\text{-VGSARAE}+H_2O+K]^+$, respectively.

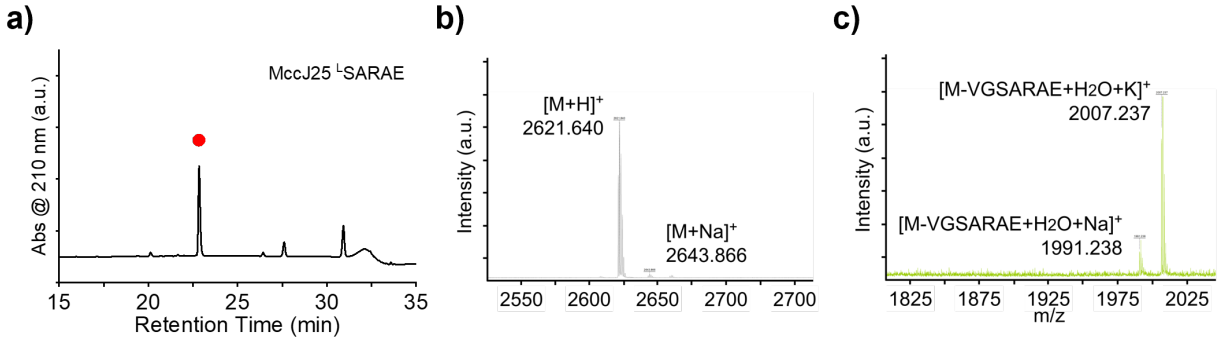

Figure S14. The HPLC analysis and MS confirmation of MccJ25 $^{L}G_2S_2G_2S_2G_2$ variant MccJ25 $^{L}G_2S_2G_2S_2G_2$ variant. **a)** Crude extract was analyzed by HPLC with $^{L}G_2S_2G_2S_2G_2$ variant eluted at t_R = 23.5 min. **b)** The peak presumed to be $^{L}G_2S_2G_2S_2G_2$ variant was collected and confirmed by MALDI-TOF MS with the observed m/z 2819.724 and 2835.710 as the sodium and potassium adduct $[M+Na]^+$ and $[M+K]^+$, respectively. **c)** Thermolysin digestion with single cleavage as the result lead to the hydrolysis of $^{L}G_2S_2G_2S_2G_2$ variant, with the observed m/z 2837.398 and 2853.382 as the sodium and potassium adduct $[M+H_2O+Na]^+$ and $[M+H_2O+K]^+$, respectively.

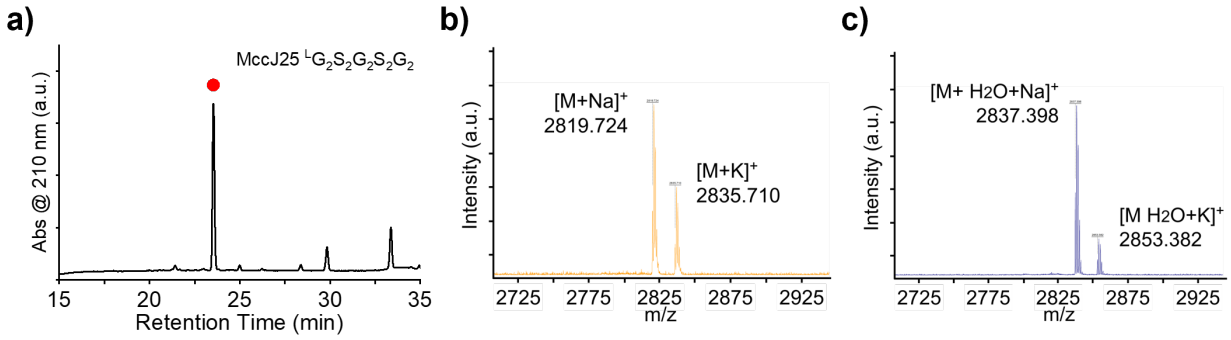

Figure S15. Lasso structure prediction for all MccJ25 variants

We used LassoPred to visualize the lasso structure of all tail- and loop-expansion variants,[9] an algorithm designed specifically for lasso peptides (https://lassopred.accre.vanderbilt.edu/). The predicted structure was presented after rending by using the PyMOL Molecular Graphics System, v.3.1 (Schrödinger LLC, USA). The ring region of all variants was colored in limegreen, the isopeptide bond between Gly1 N-terminal amine and Glu8 side-chain carboxylate in orange, and the rest of the peptide in dark gray. The loop regions of all variants adopt a similar β-hairpin-like compact structure and their tails pass through the macrolactam ring. Amino acid insertions, i.e., the "expansions", were shown in red.

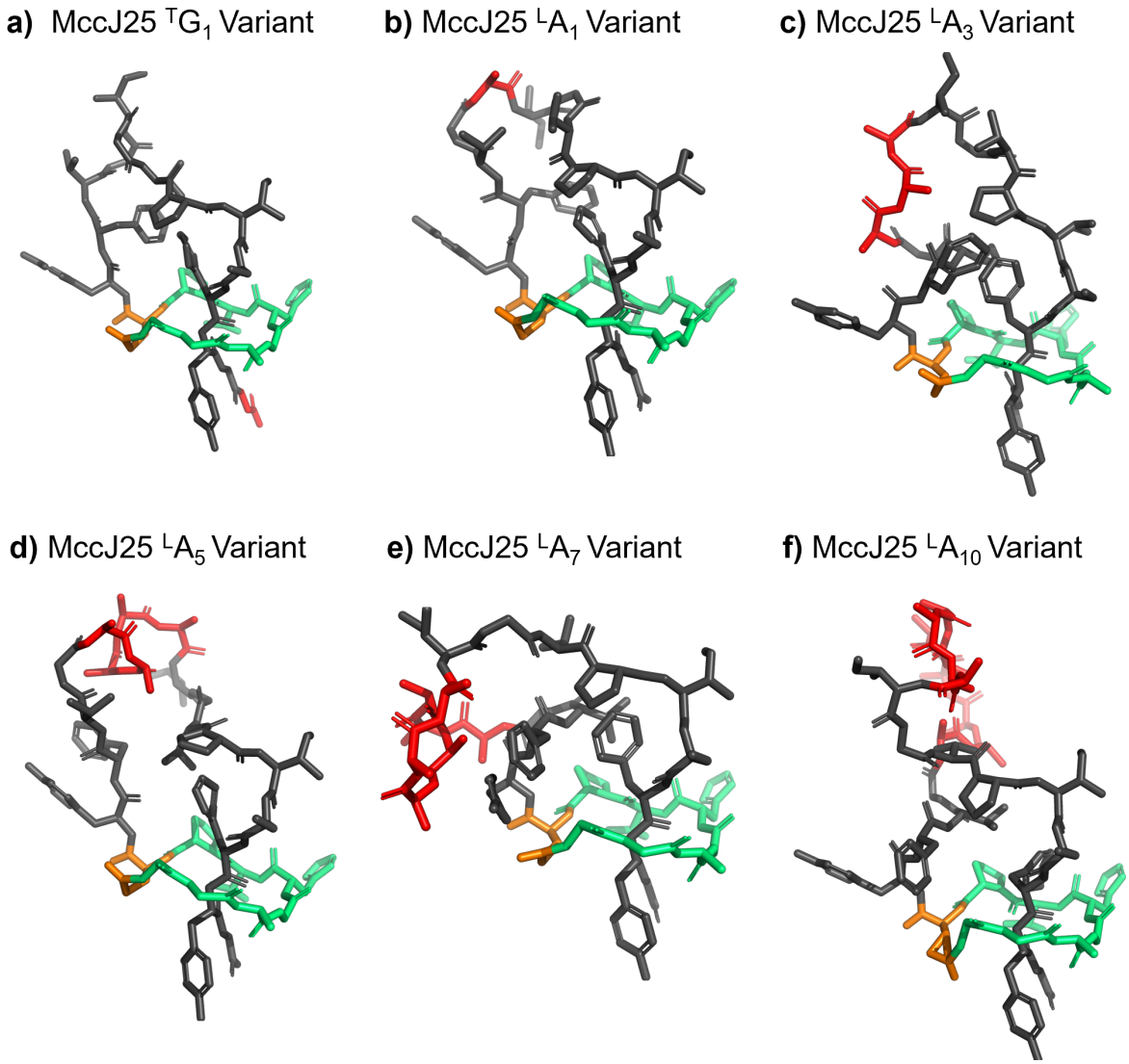

g) MccJ25 $^{L}G_{10}$ Variant

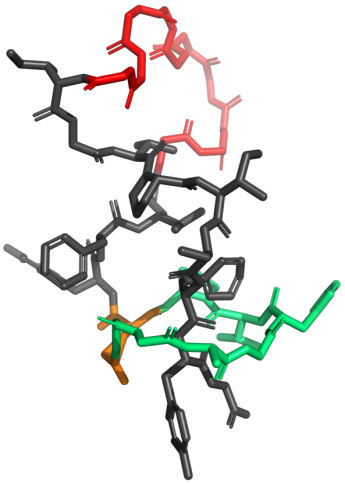

h) MccJ25 $^{L}G_{15}$ Variant

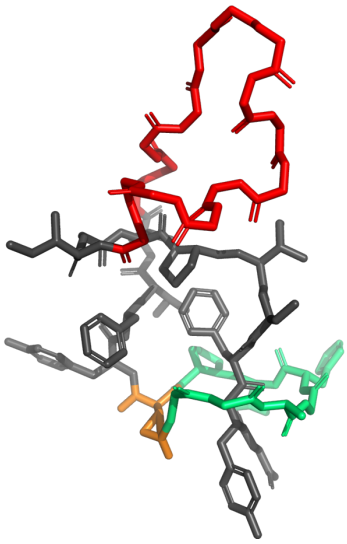

i) MccJ25 $^{L}A_1A_1$ variant

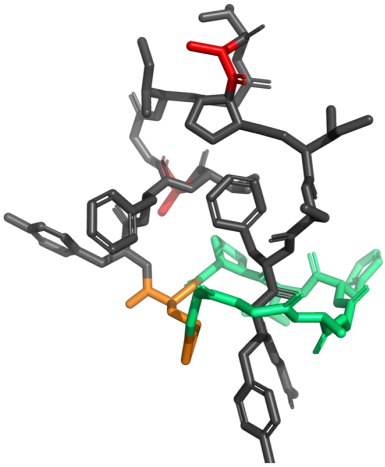

j) MccJ25 ^{L}ARA variant

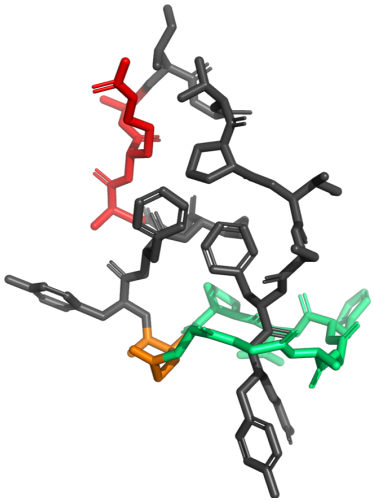

k) MccJ25 ^{L}SARAE variant

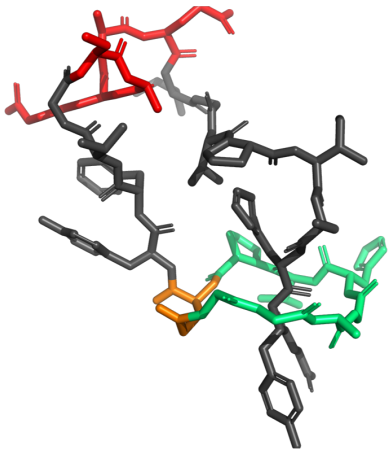

l) MccJ25 $^{L}G_2S_2G_2S_2G_2$ variant

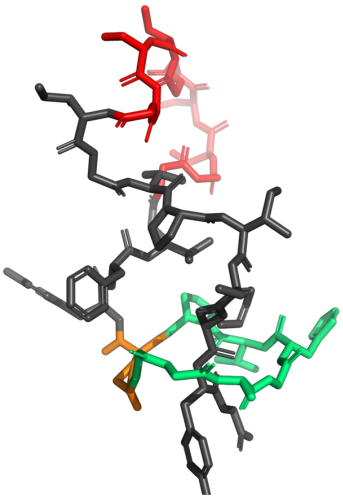

SUPPLEMENTARY TABLEs

Table S1. DNA primers used in this study

MccJ25	Name	Sequence (5' to 3')
$^{R}A_1$	mcjA_+A3_F	GCAGGACATGTGCCTGAGTATTTTG
	mcjA_+A3_R	CGCACCACCTTTTGTGAGTTGCG
$^{T}G_1$	mcjA_+G22_F	GGGTGATATTCTGAAAGAAGAACTCTGTCATTTTGTC
	mcjA_+G22_R	GCCATAGAAAGATATAGGTGTACCAATCCCC
$^{L}A_1$	mcjA_+A13_F	GCAATTGGTACACCTATATCTTTCTATGGCTGATATTC
	mcjA_+A13_R	CCCCACAAAATACTCAGGCACATG
$^{L}A_3$	mcjA_+A13_F	GCAATTGGTACACCTATATCTTTCTATGGCTGATATTC
	mcjA_+AAA_R	GGCCGCCCCCACAAAATACTCAGGCACATG
$^{L}A_5$	mcjA_+A(5)_F	GCTGCGGCAATTGGTACACCTATATCTTTCTATGGCTG
	mcjA_+AAA_R	GGCCGCCCCCACAAAATACTCAGGCACATG
$^{L}A_7$	mcjA_+A(7)_F	GCGGCTGCAATTGGTACACCTATATCTTTCTATGGCTG
	mcjA_+A(7)_R	GGCTGCAGCTGCCCCCACAAAATACTCAGGCACATG
$^{L}A_{10}$	mcjA_+A(10)_F	GCTGCTGCGGCCGCGATTGGTACACCTATATCTTTCTATGGCTGA
	mcjA_+A(10)_R	GGCTGCAGCAGCGGCCCCCACAAAATACTCAGGCACATG
$^{L}G_{10}$	mcjA_+G(10)_F	GTGGTGGAGGCGGGATTGGTACACCTATATCTTTCTATGGCTGA
	mcjA_+G(10)_R	CTCCTCCCCCGCCGCCCCCCACAAAATACTCAGGCACATG
$^{L}G_{15}$	mcjA_+G(15)_F	GAGGCGGGGGAGGTGGTGGCGGCATTGGTACACCTATATCTTTCTATGGCTGA
	mcjA_+G(15)_R	CACCACCTCCTCCCCCGCCGCCCCCCACAAAATACTCAGGCACATG
$^{L}A_1A_1$	mcjA_A12A17_F	GGTACAGCTCCTATATCTTTCTATGGCTG
	mcjA_A12A17_R	AATCCCGGCCACAAAATACTCAGG
^{L}ARA	mcjA_+A13_F	GCAATTGGTACACCTATATCTTTCTATGGCTGATATTC
	mcjA_+ARA_R	CCTTGCCCCCACAAAATACTCAGGCACATG
^{L}SARAE	mcjA_+SARAE_F	GCAGAGATTGGTACACCTATATCTTTCTATGGCTG
	mcjA_+SARAE_R	CCTTGCTGACCCCACAAAATACTCAGGCAC
$^{L}G_2S_2G_2S_2G_2$	mcjA_+GS(10)_F	GTTCTTCTGGCGGGATTGGTACACCTATATCTTTCTATGGCTGA
	mcjA_+GS(10)_R	CTCCACTACTGCCGCCCCCCACAAAATACTCAGGCACATG

Table S2. Fragmentation series of MccJ25 $^{L}G_{15}$ variant

MS^2 analysis of m/z 994.11 from Figure 2e, peptide sequences corresponding to the fragment ions are highlighted in bold.

	ion	charge	[M+H]+ calc.	[M+H]+obs.
C-terminal y-series				
GGAHGVPE**YFVGGGGGGGGGGGGGGGGIGTPISFYG**	y28	2+	1138.5147	1138.9820
GGAHGVPEYFVGGG**GGGGGGGGGGGGGIGTPISFYG**	y22	1+	1695.7725	1695.6028
GGAHGVPEYFVGGGGG**GGGGGGGGGGGIGTPISFYG**	y20	1+	1581.7295	1581.6134
GGAHGVPEYFVGGGGGG**GGGGGGGGGGIGTPISFYG**	y19	1+	1524.7081	1524.2094
GGAHGVPEYFVGGGGGGG**GGGGGGGGGIGTPISFYG**	y18	1+	1467.6866	1467.9879
GGAHGVPEYFVGGGGGGGG**GGGGGGGGIGTPISFYG**	y17	1+	1410.6651	1410.9384
GGAHGVPEYFVGGGGGGGGG**GGGGGGGIGTPISFYG**	y16	1+	1353.6437	1353.6412
GGAHGVPEYFVGGGGGGGGGG**GGGGGGIGTPISFYG**	y15	1+	1296.6222	1296.5852
GGAHGVPEYFVGGGGGGGGGGG**GGGGIGTPISFYG**	y13	1+	1182.5793	1182.4979
GGAHGVPEYFVGGGGGGGGGGGG**GGGIGTPISFYG**	y12	1+	1125.5578	1125.4789
GGAHGVPEYFVGGGGGGGGGGGGG**GGIGTPISFYG**	y11	1+	1068.5364	1068.4590
GGAHGVPEYFVGGGGGGGGGGGGGGG**IGTPISFYG**	y9	1+	954.4934	954.6899
GGAHGVPEYFVGGGGGGGGGGGGGGGI**GTPISFYG**	y8	1+	841.4094	841.3467
GGAHGVPEYFVGGGGGGGGGGGGGGGIG**TPISFYG**	y7	1+	784.3879	784.3349
GGAHGVPEYFVGGGGGGGGGGGGGGGIGT**PISFYG**	y6	1+	683.2402	683.3266
GGAHGVPEYFVGGGGGGGGGGGGGGGIGTP**ISFYG**	y5	1+	586.2875	586.2806
GGAHGVPEYFVGGGGGGGGGGGGGGGIGTPI**SFYG**	y4	1+	473.2034	473.1899
GGAHGVPEYFVGGGGGGGGGGGGGGGIGTPIS**FYG**	y3	1+	386.1714	386.1682
GGAHGVPEYFVGGGGGGGGGGGGGGGIGTPISF**YG**	y2	1+	239.1030	239.0999
N-terminal b-series				
GGAHGVPEYFVGGGGGGGGGGGGGGGGIGTPISFYG	b8	1+	687.3318	687.3102
GGAHGVPEYFVGGGGGGGGGGGGGGGGIGTPISFYG	b9	1+	850.3875	850.1786
GGAHGVPEYFVGGGGGGGGGGGGGGGGIGTPISFYG	b10	1+	997.4635	997.4217
GGAHGVPEYFVGGGGGGGGGGGGGGGGIGTPISFYG	b11	1+	1096.5243	1096.4852
GGAHGVPEYFVGGGGGGGGGGGGGGGGIGTPISFYG	b12	1+	1153.6468	1153.4940
GGAHGVPEYFVGGGGGGGGGGGGGGGGIGTPISFYG	b13	1+	1210.5673	1210.6631
GGAHGVPEYFVGGGGGGGGGGGGGGGGIGTPISFYG	b14	1+	1267.5887	1267.5243
GGAHGVPEYFVGGGGGGGGGGGGGGGGIGTPISFYG	b15	1+	1324.6102	1324.5673
GGAHGVPEYFVGGGGGGGGGGGGGGGGIGTPISFYG	b16	1+	1381.6317	1381.2921

GGAHGVPEYFVGGGGGGGGGGGGGGGGIGTPISFYG	b17	2+	719.8266	719.8044
GGAHGVPEYFVGGGGGGGGGGGGGGGGGIGTPISFYG	b18	1+	1495.6746	1495.7456
GGAHGVPEYFVGGGGGGGGGGGGGGGGGGIGTPISFYG	b19	1+	1552.6961	1552.0441
GGAHGVPEYFVGGGGGGGGGGGGGGGGGIGTPISFYG	b21	2+	833.8695	833.4049
GGAHGVPEYFVGGGGGGGGGGGGGGGGIGTPISFYG	b24	2+	919.4017	919.9049
GGAHGVPEYFVGGGGGGGGGGGGGGGGIGTPISFYG	b29	2+	1089.9867	1089.9494
GGAHGVPEYFVGGGGGGGGGGGGGGGGGIGTPISFYG	b30	2+	1140.5105	1140.4925
GGAHGVPEYFVGGGGGGGGGGGGGGGGGIGTPISFYG	b31	3+	793.0322	793.3274
GGAHGVPEYFVGGGGGGGGGGGGGGGGGIGTPISFYG	b32	3+	830.7269	830.6906

Sterically linked by y-series

GGAHGVPE(YF)**VGGGGGGGGGGGGGGGGGIGTPISFYG**	b8+y26	3+	884.7406	884.9957
GGAHGVPE(YFV)**GGGGGGGGGGGGGGGGGIGTPISFYG**	b8+y25	3+	851.7178	851. 6890
GGAHGVPE(YFVGG)**GGGGGGGGGGGGGGGGIGTPISFYG**	b8+y23	3+	813.7035	813.0065
GGAHGVPE(YFVGGG)**GGGGGGGGGGGGGGGIGTPISFYG**	b8+y22	3+	794.6964	794.6284
GGAHGVPE(YFVGGGGGG)**GGGGGGGGGGIGTPISFYG**	b8+y19	3+	737.6749	737.9854
GGAHGVPE(YFVGGGGGGGG)**GGGGGGGGGIGTPISFYG**	b8+y17	3+	699.6606	699.4940
GGAHGVPE(YFVGGGGGGGGG)**GGGGGGGGIGTPISFYG**	b8+y16	3+	680.6534	680.4859
GGAHGVPE(YFVGGGGGGGGGG)**GGGGGGGIGTPISFYG**	b8+y15	2+	991.9694	991.5682
GGAHGVPE(YFVGGGGGGGGGGG)**GGGGGIGTPISFYG**	b8+y13	2+	934.9480	934.6476
GGAHGVPE(YFVGGGGGGGGGGGGG)**GGIGTPISFYG**	b8+y11	2+	877.9265	877.3660
GGAHGVPE(YFVGGGGGGGGGGGGGG)**GIGTPISFYG**	b8+y10	2+	849.4158	849.8871
GGAHGVPE(YFVGGGGGGGGGGGGGGG)**IGTPISFYG**	b8+y9	1+	1697.8315	1697.8713
GGAHGVPE(YFVGGGGGGGGGGGGGGGI)**GTPISFYG**	b8+y8	1+	1527.7260	1527.6676
GGAHGVPE(YFVGGGGGGGGGGGGGGGIG)**TPISFYG**	b8+y7	2+	735.8523	735.8329
GGAHGVPE(YFVGGGGGGGGGGGGGGGIGT)**PISFYG**	b8+y6	1+	1369.5568	1369.6429
GGAHGVPE(YFVGGGGGGGGGGGGGGGIGTP)**ISFYG**	b8+y5	1+	1272.6041	1272.5318
GGAHGVPE(YFVGGGGGGGGGGGGGGGIGTPI)**SFYG**	b8+y4	1+	1159.5200	1159.4993
GGAHGVPEY(FV)**GGGGGGGGGGGGGGGGGIGTPISFYG**	b9+y25	3+	906.0723	906.0188
GGAHGVPEY(FVGG)**GGGGGGGGGGGGGGGIGTPISFYG**	b9+y23	3+	868.0579	868.5702
GGAHGVPEY(FVGGGG)**GGGGGGGGGGGGGGIGTPISFYG**	b9+y21	3+	830.0436	830.3635
GGAHGVPEY(FVGGGGGG)**GGGGGGGGGGGGIGTPISFYG**	b9+y19	3+	792.0293	792.9862
GGAHGVPEY(FVGGGGGGG)**GGGGGGGGGGIGTPISFYG**	b9+y18	3+	773.0222	773.6485
GGAHGVPEY(FVGGGGGGGGG)**GGGGGGGIGTPISFYG**	b9+y16	3+	735.0079	735.0003
GGAHGVPEY(FVGGGGGGGGGG)**GGGGGGGIGTPISFYG**	b9+y15	2+	1073.5010	1073.9351
GGAHGVPEY(FVGGGGGGGGGGG)**GGGGGGIGTPISFYG**	b9+y14	3+	696.9936	696.1173

GGAHGVPEY(FVGGGGGGGGGGGGGGGGI)**GTPISFYG**	b9+y8	2+	845.8947	845.9002
GGAHGVPEY(FVGGGGGGGGGGGGGGGGIGT)**PISFYG**	b9+y6	1+	1532.6201	1532.6168
GGAHGVPEY(FVGGGGGGGGGGGGGGGGIGTP)**ISFYG**	b9+y5	1+	1435.6674	1435.6002
GGAHGVPEY(FVGGGGGGGGGGGGGGGGIGTPI)**SFYG**	b9+y4	1+	1322.5833	1322.5402
GGAHGVPEYF(VGG)**GGGGGGGGGGGGGGIGTPISFYG**	b10+y23	3+	917.0807	917.7498
GGAHGVPEYF(VGGGG)**GGGGGGGGGGGGGIGTPISFYG**	b10+y21	3+	879.0664	879.0642
GGAHGVPEYF(VGGGGGGGGGGGG)**GGGGIGTPISFYG**	b10+y13	2+	1090.0140	1090.4257
GGAHGVPEYF(VGGGGGGGGGGGGGGGGI)**GTPISFYG**	b10+y8	2+	919.4289	919.2049
GGAHGVPEYF(VGGGGGGGGGGGGGGGGIGT)**PISFYG**	b10+y6	1+	1679.6885	1679.7903
GGAHGVPEYF(VGGGGGGGGGGGGGGGGIGTP)**ISFYG**	b10+y5	1+	1582.7358	1582.6563
GGAHGVPEYF(VGGGGGGGGGGGGGGGGIGTPI)**SFYG**	b10+y4	2+	735.3259	735.3261

REFERENCEs

[1] Solbiati JO, Ciaccio M, Farías RN, Salomón RA. Genetic analysis of plasmid determinants for microcin J25 production and immunity. *J Bacteriol*., **1996**, *178*

[2] P. H. Chen, L. K. Sung, J. D. Hegemann, J. Chu. Disrupting transcription and folate biosynthesis leads to synergistic suppression of Escherichia coli growth. *ChemMedChem* **2022**, *17*, e202200075

[3] Tan, H. N.; Liu, W. Q.; Ho, J.; Chen, Y. J.; Shieh, F. J.; Liao, H. T.; Wang, S. P.; Hegemann, J. D.; Chang, C. Y.; Chu, J. Structure prediction and protein engineering yield new insights into microcin J25 precursor recognition. *ACS Chem Biol*. **2024**, *43*, 4696-702

[4] Abramson, J., Adler, J., Dunger, J. et al. Accurate structure prediction of biomolecular interactions with AlphaFold 3. *Nature* **2024**, *630*, 493–500.

[5] AlphaFold server. https://alphafoldserver.com/ (accessed March 13, 2026)

[6] Ye, B.; Tian, W.; Wang, B.; Liang, J. CASTpFold: Computed Atlas of Surface Topography of the universe of protein Folds, *Nucleic Acids Research*, **2024**, *52*, W1, 194–199

[7] CASTpFold server. https://cfold.bme.uic.edu/castpfold/compute (accessed March 13, 2026)

[8] Ducasse, R.; Yan, K. P.; Goulard, C.; Blond, A.; Li, Y.; Lescop, E.; Guittet, E.; Rebuffat, S.; Zirah, S.; Sequence determinants governing the topology and biological activity of a lasso peptide, microcin J25. *ChemBioChem* **2012**, *13*, 371-80

[9] Ouyang, X., Ran, X., Xu, H. *et al*. LassoPred: a tool to predict the 3D structure of lasso peptides. *Nat Commun* **2025**, *16*, 5497